BBA - Molecular Basis of Disease 1865 (2019) 165536

Contents lists available at ScienceDirect

BBA - Molecular Basis of Disease

journal homepage: www.elsevier.com/locate/bbadis

Characterization of the C584R variant in the mtDNA depletion syndrome gene FBXL4, reveals a novel role for FBXL4 as a regulator of mitochondrial fusion

Rasha Sabouny[a,e,*], Rachel Wong[e], Laurie Lee-Glover[e], Steven C. Greenway[a,c,d,e,g], David S. Sinasac[b,e], Care4Rare Canada, Aneal Khan[b,c,e], Timothy E. Shutt[a,b,e,f,**]

[a] Department of Biochemistry & Molecular Biology, Cumming School of Medicine, University of Calgary, Calgary, AB, Canada
[b] Department of Medical Genetics, Cumming School of Medicine, University of Calgary, Calgary, AB, Canada
[c] Department of Pediatrics, Cumming School of Medicine, University of Calgary, Calgary, AB, Canada
[d] Department of Cardiac Sciences, Cumming School of Medicine, University of Calgary, Calgary, AB, Canada
[e] Alberta Children's Hospital Research Institute, University of Calgary, Calgary, Alberta, Canada
[f] Hotchkiss Brain Institute, University of Calgary, Calgary, Alberta, Canada
[g] Libin Cardiovascular Institute of Alberta, University of Calgary, Calgary, Alberta, Canada

ARTICLE INFO

Keywords:
Mitochondria
Mitochondrial DNA depletion
Mitochondrial fusion
FBXL4
Dichloroacetate

ABSTRACT

Mutations in *FBXL4* (F-Box and Leucine rich repeat protein 4), a nuclear-encoded mitochondrial protein with an unknown function, cause mitochondrial DNA depletion syndrome. We report two siblings, from consanguineous parents, harbouring a previously uncharacterized homozygous variant in *FBXL4* (c.1750 T > C; p.Cys584Arg). Both patients presented with encephalomyopathy, lactic acidosis and cardiac hypertrophy, which are reported features of FBXL4 impairment. Remarkably, dichloroacetate (DCA) administration to the younger sibling improved metabolic acidosis and reversed cardiac hypertrophy. Characterization of FBXL4 patient fibroblasts revealed severe bioenergetic defects, mtDNA depletion, fragmentation of mitochondrial networks, and abnormalities in mtDNA nucleoids. These phenotypes, observed with other pathogenic *FBXL4* variants, confirm the pathogenicity of the p.Cys584Arg variant. Although treating FBXL4 fibroblasts with DCA improved extracellular acidification, in line with reduced lactate levels in patients, DCA treatment did not improve any of the other mitochondrial functions. Nonetheless, we highlight DCA as a potentially effective drug for the management of elevated lactate and cardiomyopathy in patients with pathogenic *FBXL4* variants. Finally, as the exact mechanism through which *FBXL4* mutations lead to mtDNA depletion was unknown, we tested the hypothesis that FBXL4 promotes mitochondrial fusion. Using a photo-activatable GFP fusion assay, we found reduced mitochondrial fusion rates in cells harbouring a pathogenic *FBXL4* variant. Meanwhile, overexpression of wildtype FBXL4, but not the p.Cys584Arg variant, promoted mitochondrial hyperfusion. Thus, we have uncovered a novel function for FBXL4 in promoting mitochondrial fusion, providing important mechanistic insights into the pathogenic mechanism underlying *FBXL4* dysfunction.

Abbreviations: ATP5A, ATP Synthase Subunit Alpha; COX II, Cytochrome c oxidase subunit 2; DCA, Dichloroacetate; DGUOK, Deoxyguanosine Kinase; DMEM, Dulbecco's Modified Eagle Medium; dNTP, Deoxyribonucleotide triphosphate; DRP1, Dynamin Related Protein 1; ECAR, Extracellular Acidification Rate; FBXL4, F-Box and Leucine rich repeat 4; FCCP, Carbonyl cyanide 4-(trifluoromethoxy) phenylhydrazone; GFP, Green Fluorescent Protein; HA, Hemagglutinin; HEK, Human Embryonic Kidney; HEPES, 4-(2-hydroxyethyl)-1-piperazineethanesulfonic acid); HSP60, Heat Shock Protein 60; IMS, Intermembrane Space; IVSd, Interventricular Septum Thickness; MELAS, Mitochondrial encephalomyopathy, lactic acidosis, and stroke-like episodes; MEM, Minimum Essential Media; MFN1/2, Mitofusin1/2; mtDNA, Mitochondrial deoxyribonucleic acid; MTO1, Mitochondrial Translation Optimization 1; NDUFB8, NADH:Ubiquinone Oxidoreductase Subunit B8; OCR, Oxygen Consumption Rate; OMIM, Online Mendelian Inheritance in Man; OPA1, Optic Atrophy 1; OXPHOS, Oxidative Phosphorylation; PA-GFP, Photoactivatable Green Fluorescent Protein; PBS, Phosphate Buffered Saline; PDHC, Pyruvate Dehydrogenase Complex; POLG, Polymerase Gamma; QPCR, Quantitative Polymerase Chain Reaction; RRM2B, Ribonucleotide Reductase Regulatory TP53 Inducible Subunit M2B; SDHB, Succinate Dehydrogenase Complex Iron Sulfur Subunit B; SUCLA2, Succinate-CoA Ligase ADP-Forming Beta Subunit; SUCLG1, Succinate-CoA Ligase Alpha Subunit; TK2, Thymidine Kinase 2; TMRE, Tetramethylrhodamine, ethyl ester; TWNK, Twinkle; TYMP, Thymidine Phosphorylase; UQCRC2, Ubiquinol-Cytochrome C Reductase Core Protein 2

* Correspondence to: R. Sabouny, Department of Biochemistry & Molecular Biology, Cumming School of Medicine, University of Calgary, Calgary, AB, Canada.
** Correspondence to: T. E Shutt, Department of Medical Genetics, Cumming School of Medicine, University of Calgary, Calgary, AB, Canada.
E-mail addresses: rasha.sabouny@ucalgary.ca (R. Sabouny), timothy.shutt@ucalgary.ca (T.E. Shutt).

https://doi.org/10.1016/j.bbadis.2019.165536
Received 1 March 2019; Received in revised form 16 July 2019; Accepted 18 August 2019
Available online 20 August 2019

1. Introduction

FBXL4 (F-Box and Leucine rich repeat protein 4) is a nuclear-encoded mitochondrial protein proposed to localize to the mitochondrial intermembrane space (IMS) [1]. Although mutations in *FBXL4* cause a mitochondrial DNA (mtDNA) depletion syndrome with infant-onset encephalopathy and lactic acidosis (OMIM 615471, [2]) [1,3–12], the exact function of the FBXL4 protein has remained elusive. Thus, we do not have a clear understanding of how FBXL4 impairment leads to disease. MtDNA depletion syndromes are a subclass of mitochondrial disease with genetic and phenotypic heterogeneity, which are characterized by significant reduction of mtDNA content in affected tissues [13,14]. MtDNA depletion syndromes are typically caused by mutations in nuclear-encoded genes that support mtDNA replication (e.g., *POLG* and *TWNK*) or maintenance of mitochondrial deoxyribonucleotide triphosphate (dNTP) pools (e.g., *TK2*, *DGUOK*, *RRM2B*, *TYMP*, *SUCLA2* and *SUCLG1*) [13,14]. However, mounting evidence suggests that dysregulation of mitochondrial fusion can also cause mtDNA depletion in mitochondrial disease patients [15–19]. To date, *FBXL4* is one of the few mtDNA depletion syndrome genes with an unknown pathogenesis mechanism [13,14].

Fusion and fission events constantly remodel mitochondrial shape, which can range from connected reticular networks to fragmented puncta [20,21]. Importantly, changes to mitochondrial morphology encompass redistribution of mitochondrial contents, including mtDNA nucleoids (nucleoprotein structures into which mtDNA is packaged) [22–25]. Mitochondrial fission is mainly driven by the GTPase Dynamin Related protein 1 (DRP1) [26]. Meanwhile, fusion of mitochondrial membranes is also regulated by large GTPases namely, Mitofusin 1 and 2 (MFN1/2) at the outer mitochondrial membrane, and Optic Atrophy 1 protein (OPA1) at the inner mitochondrial membrane [26]. Cells lacking any of the core fusion proteins contain not only fragmented mitochondrial networks, but also abnormal distribution of mtDNA nucleoids and mtDNA genome instability [25]. Moreover, pathogenic mutations in *MFN2* and *OPA1* genes have been reported to cause mtDNA depletion in patients [15–19]. Nevertheless, we still do not have a complete understanding of how impaired fusion causes mtDNA depletion.

Early onset, multisystemic presentation is characteristic of mtDNA depletion syndromes, and in the absence of effective therapeutics, poor prognosis is projected if symptoms are left unmanaged. Lactic acidemia is a common metabolic problem among mitochondrial disease patients, especially in patients carrying pathogenic *FBXL4* variants [1,3–12]. One way to tackle elevated lactate levels is by administering dichloroacetate (DCA), a glycolysis inhibitor that functions by inhibiting pyruvate dehydrogenase kinase, leading to activation of the pyruvate dehydrogenase complex (PDHC) [27,28]. Ultimately, activating PDHC prevents the conversion of pyruvate to lactate, and thus reduces lactate accumulation in blood and tissues [27,28].

Herein, we report two siblings harbouring a previously uncharacterized homozygous mutation in *FBXL4* (c.1750 T > C; p.Cys584Arg, hereafter referred to as C584R), and exhibiting characteristic phenotypes of FBXL4 dysfunction. Notably, the second patient, who was treated with DCA, showed improved lactate levels and reversal of cardiac hypertrophy. We set out to characterize patient fibroblasts harbouring the C584R mutation and confirm the pathogenic nature of this variant. In addition, as no effective treatment has been reported for FBXL4 impairment, we examined whether DCA improved the underlying mitochondrial function. Finally, we wanted to test the hypothesis that FBXL4 promotes mitochondrial fusion, which would explain the mtDNA depletion in these patients.

2. Materials and methods

The sequencing component of this work was part of Care for Rare (http://care4rare.ca) and the tissue analysis was part of the MITO-FIND project (mitochondrial functional and integrative next generation diagnostics) sponsored by MitoCanada (http://mitocanada.org). For both projects, consent was obtained following standard procedures through the University of Calgary Conjoint Research Ethics Board.

2.1. Cell culture

Control and patient primary fibroblasts (from skin or muscle biopsies, obtained with informed consent) were cultured in MEM media (Gibco, 11095080) containing L-Glutamine and supplemented with 10% fetal bovine serum (FBS) and 1 mM sodium pyruvate. Where indicated, fibroblasts were treated with 10 mM DCA (Sigma Aldrich, 347795) for 24 h, or 25 μM mdivi-1 (Sigma Aldrich, M0199) for 24 h or 1 week. HEK cells were grown in DMEM (Gibco, 11965092) supplemented with 10% FBS. Cells were maintained at 37 °C and 5% CO_2.

Overexpression of PA-GFP in fibroblasts was mediated by electroporation using the Amaxa Nucleofector II system (Lonza). The mito-PAGFP was a gift from Richard Youle (Addgene plasmid # 23348; http://n2t.net/addgene:23348; RRID: Addgene_23348) [29]. Cells were harvested and resuspended in OptiMEM media, counted and prepared at 1×10^6 cells per 100 μL. The cell suspension, including 2 μg of the plasmid, was then transferred to a sterile 2 mm electroporation cuvette (VWR 89047-208) and electroporated using the A-024 program on the Nucleofector device. Electroporated cells were subsequently seeded onto glass bottom dishes (Mattek, P35G-1.5) in complete medium and maintained at 37 °C and 5% CO_2. Fresh culture media was added after 12–16 h and cells were incubated until ready for imaging.

For overexpression studies, HEK cells were transfected with a mammalian expression vector containing C-terminal HA-tagged FBXL4 (a generous gift from Dr. Zeviani) using Lipofectamine 3000 (Thermo Fisher Scientific, L3000015) according to manufacturer's instructions. The original plasmid was cloned into a pcDNA3.1-backbone using InFusion cloning (Takara, Clonetech), and the C584R mutation was introduced using mutagenesis primers. For transfections, cells were seeded at 3.6×10^5 in 6-well plates and allowed to grow overnight. The following day, 2 μg of plasmid were used for transfections and cells were left to grow for 24 h before harvesting/fixation.

2.2. mtDNA copy number analysis

Genomic DNA (nuclear and mitochondrial DNA) was isolated from control and patient fibroblasts (seeded at 5×10^5 cells) using the PureLink Genomic DNA Mini Kit (Thermo Fisher Scientific, K182001) according to manufacturer's instructions. The QuantStudio 6 Flex Real-Time PCR system (Thermo Fisher Scientific) was used to assess relative mtDNA copy number. Primer sequences to amplify mtDNA and the nuclear-encoded housekeeping gene 18S, and thermocycling conditions were exactly as described in [30]. Briefly, the 20 μL quantitative PCR (QPCR) reactions contained 10 μL PowerUp SYBR Green Master Mix (Thermo Fisher Scientific, A25742), 100 ng gDNA and 500 nM forward and 500 nM reverse primers (final concentrations). MtDNA copy number relative to 18S was analyzed using the delta delta Ct method and represented as percent control [31]. Reactions were performed in triplicate and mtDNA copy number analysis was performed on at least three independent biological replicates. Data is presented as mean ± SD and unpaired, 2-tailed Student's *t*-tests were used to determine statistical significance.

2.3. Western blot

For Western analyses, 5×10^5 cells were seeded in 100 mm plates, and allowed to grow for 2 days. Cells were harvested by trypsinization, pelleted, washed with 1× phosphate buffered saline (PBS) and lysed with RIPA buffer containing protease inhibitors. Total cell lysates were resolved on SDS-PAGE gels and transferred onto PVDF membranes. For analyses examining expression of OXPHOS subunits, 50 μg total cell

lysates were loaded, meanwhile for all other Western analyses, 20 μg protein was used. Blots were probed with the following antibodies at 1:1000 dilution: OXPHOS antibody cocktail (Abcam, ab110411), anti-MFN1 (Cell Signalling, 14739), anti-MFN2 (Abnova, H00009927-M03), anti-OPA1 (BD Bioscience, 612606), anti-DRP1 (BD Bioscience, 611113), anti-Actin (Sigma, A5316), anti-HSP60 (Cell Signalling, 12165), anti-tubulin (Santa Cruz Biotechnology, D-10) and the appropriate horseradish peroxidase (HRP)-conjugated secondary antibodies (1:3000). Blots were incubated with Clarity ECL substrate (Biorad, 1705061) and imaged using an Amersham Imager AI600.

2.4. Mitochondrial respiration

The Seahorse XFe24 Extracellular Flux Analyzer (Agilent Technologies, Inc) was used to examine mitochondrial bioenergetic profiles in control and patient fibroblasts as described in [32]. Briefly, 3.75×10^4 cells/well were seeded in an XF24 microplate and incubated at 37 °C, 5% CO_2 for 24 h. Next, DCA (10 mM) was added where indicated and the cells were allowed to grow for another 24 h. Subsequently, growth media was replaced with assay media supplemented with D-Glucose (25 mM), sodium pyruvate (2 mM) and L-Glutamine (4 mM). Oxygen consumption rates were measured following sequential injection of the following compounds into each well: oligomycin (1 μg/mL) (Enzo Life Sciences, BML-CM111), carbonyl cyanide 4-(trifluoromethoxy) phenylhydrazone (FCCP, 1 μM) (Enzo life Sciences, BML-CM120) and Antimycin A (1 μM) (Sigma Aldrich, A8674). Upon completion of the assay, assay media was aspirated, wells were carefully washed with 1XPBS and 15 μL of RIPA buffer were added. Protein concentrations from each well were measured by BCA assay (Thermo Fisher Scientific, 23225) and used to normalize data.

2.5. Immunofluorescence staining

Fibroblasts were seeded on 12 mm glass coverslips (no. 1.5) at 2×10^4 cells and incubated for 1–2 days. Subsequently, cells were fixed and stained with primary antibodies against TOMM20 (Santa Cruz Biotechnology, FL-145 or F-10), DNA (Millipore, CBL186), HA (Santa Cruz Biotechnology, F-7) and appropriate Alexafluor-conjugated secondary antibodies (Thermo Fisher Scientific) at 1:1000 as previously described [32].

2.6. Live cell staining

Fibroblasts were seeded on 35 mm glass bottom dishes at 8×10^4 and incubated overnight. Prior to imaging, cells were simultaneously stained with MitoTracker Red dye (50 nM) (Thermo Fisher Scientific, M7512) and PicoGreen (Thermo Fisher Scientific, P7581) (3 μL/mL as in [33]) to visualize mitochondrial networks and mtDNA nucleoids, respectively. After 30–45 min incubation at 37 °C, the media containing dyes was aspirated, cells were washed with pre-warmed 1XPBS and fresh media was added. Additionally, 10 mM HEPES buffer was added prior to imaging.

Similarly, where indicated, cells were stained with the membrane potential-dependent dye TMRE (Tetramethylrhodamine, ethyl ester) (50 nM, 20 min) (Life Technologies, T669) as above, washed with 1XPBS and replenished with pre-warmed media and 10 mM HEPES buffer.

2.7. Microscopy

Fixed samples were imaged on an Olympus spinning disc confocal system (Olympus SD OSR) (UAPON 100XOTIRF/1.49 oil objective) operated by Metamorph software. Live cell imaging was performed on a line scanning confocal microscope (Zeiss LSM 700) (40X/1.4 oil objective) operated by Zen software. Live cells were maintained at 37 °C for the duration of imaging and media was buffered with HEPES.

2.8. Photo-activatable GFP fusion assay

Fibroblasts transfected with a matrix-targeted PA-GFP and stained with TMRE were imaged on the Zeiss LSM system to assess fusion rates. For photo-activation, the 405 nm laser at 10% power was used to photoactivate a region of the mitochondrial network (approximately 5x5μm). An image was acquired pre-photoactivation, 5 s post-photoactivation and dynamic changes in mitochondrial networks were subsequently recorded at 120 s intervals (up to 960 s) using the 488 nm and 561 nm lasers.

2.9. Image analysis

2.9.1. Mitochondrial networks

Mitochondrial network morphology was qualitatively analyzed by classifying networks into three categories, fragmented (predominantly small mitochondrial fragments), Intermediate (cells containing a mixture of short fragments and elongated networks) and fused (elongated, interconnected networks with few to no short fragments). For each fibroblast or transfected HEK line, at least 50 cells were scored. Morphology analyses were performed on 3 independent replicates, the results represent mean ± SD, and *P* values were based on unpaired, 2-tailed Student's *t*-tests.

2.9.2. MtDNA nucleoids

Mitochondrial DNA nucleoid size and number were analyzed using the particle analysis tool in ImageJ FIJI [34]. Fibroblasts from fixed cells stained with an anti-DNA antibody (*Z*-stack), or live cells stained with PicoGreen (single plain) were imaged using the indicated acquisition parameters, and images were subsequently scaled and binarized. A region of interest containing the entire mitochondrial network was selected. In binarized mtDNA nucleoid images, the particle analysis tool was used to measure surface area and total nucleoid counts within the selected cell (nuclear signal was excluded). The analyses were performed on 10 fibroblasts for each patient and control lines. Nucleoid sizes are presented as the average size of all nucleoids per cell ± SD. Nucleoid counts represent mean ± SD and *P* values were based on unpaired, 2-tailed Student's *t*-tests.

2.9.3. Mitochondrial fusion analysis

Mitochondrial fusion rates were assessed in control and patient fibroblasts expressing the matrix-targeted PA-GFP by two methods; examining 1) diffusion of the GFP signal and 2) mean fluorescence intensity of GFP signal overtime. Firstly, the diffusion of the GFP signal was assessed by comparing the percentage of the network that was photoactivated at 5 s to the percentage of the network containing GFP signal at the final acquisition frame ($t = 960$ s). Images in the GFP and TMRE channels were binarized and the area of mitochondrial network in the GFP channel relative to the total network in the TMRE channel was measured at each timepoint. Wider diffusion of the GFP signal throughout the network is indicative of higher fusion rates. Representative binarized images used for these analyses are appended in Supplementary Fig. 3. Analyses were performed using ImageJ FIJI and data represent the average ± SD from 5 cells for each fibroblast line. Unpaired, student's *t*-tests were used to assess statistical significance.

Secondly, mean fluorescence intensity in the photo-activated region (5 × 5μm box) was recorded over the acquisition period using Zen Black software, as done previously [35]. A reduction in fluorescence intensity overtime is suggestive of higher fusion rates as the GFP signal spreads throughout the network. Notably, acquisition parameters were optimized to minimize photo-bleaching of the GFP and TMRE signals.

2.10. Mitochondrial membrane potential and mitochondrial mass analyses

Control and patient fibroblasts were seeded in 6-well plates at

1.5×10^5 cells per well and incubated for 1–2 days. On the day of analysis, cells were stained with TMRE (50 nM, 20 min) to examine mitochondrial membrane potential. The ionophore FCCP (Carbonylcyanide-4-(trifluoromethoxy)-phenylhydrazone, 10uM) (Enzo Life Sciences, BML-CM120) was used as a negative control. To evaluate mitochondrial mass, another set of cells were seeded as above and labelled with the membrane potential-independent dye MitoTracker Green (50 nM, 20 min) (Life technologies, M7514). After staining, cells were washed three times with pre-warmed PBS, trypsinized and pelleted. Cell pellets were resuspended in complete media and the BD LSR II flow cytometer supported by the BD FACSDiva software (BD Biosciences) was used to measure signal intensity from the respective dyes. Mean fluorescence intensity was recorded for approximately 20,000 events in triplicates of each fibroblast line. Results are presented as percent control and Unpaired Student's *t*-tests were used to assess statistical significance.

3. Results

3.1. Clinical description

We report two siblings (hereafter referred to as P1 and P2) from a consanguineous family of Arab descent with three healthy children and three miscarriages (Fig. 1A). The probands presented with encephalomyopathy, developmental delay, severe lactic acidosis and hypertrophic cardiomyopathy, suggestive of mitochondrial disease. P1, the older female sibling died at 7 months of age.

P2, the younger male sibling, was investigated more closely and showed features of polymicrogyria, cryptorchidism, chronic hydronephrosis, and cerebellar hypoplasia. Metabolic investigations in P2 showed an elevated plasma lactate:pyruvate ratio (lactate 9.5 mmol/L, pyruvate 0.23 mmol/L, L:P ratio 41; reference < 25), and elevated urinary 3-methyl glutaconic acid of 18.2 mmol/mol creatinine (reference 1.9–9.1). In addition, electron transport chain activity was globally reduced in muscle tissue, and muscle pathology was abnormal as detailed previously, prior to exome sequencing, as Case 1 in Sarnat et al., [36]. P2 died at 2 years and 10 months of age after being transferred to palliative care owing to a respiratory infection that was secondary to the disease.

3.2. Dichloroacetate (DCA) improved lactic acidosis and cardiac hypertrophy in patient 2

Based on the suspected mitochondrial disease in the first affected sibling (P1), P2 received vitamin D (600 IU/day), vitamin B1 (10 mg/kg/day), CoQ10 (10 mg/kg/day) and propranolol starting at birth. In response to increasing blood lactate levels, administration of dichloroacetate (DCA; TCI America) was started at 6 weeks of age in the dose range between 25 and 50 mg/kg/day (Fig. 1B). The clinical experience showed doses above 25 mg/kg/day were needed to reduce blood lactate levels with dosing changes adjusted for increasing weight. Remarkably, septal hypertrophy also normalized after DCA administration was initiated, with echocardiography showing no ventricular hypertrophy at 18 months of age (Fig. 1C). It is worth noting that DCA dosage was not adjusted after P2 was transferred to palliative care, hence the observed elevation in venous lactate later in life (Fig. 1B).

3.3. Genetic studies identify homozygous variants in FBXL4

Mitochondrial DNA (mtDNA) from muscle DNA was fully sequenced in P2, but no mutations or deletions were detected. Meanwhile, whole exome sequencing revealed a novel homozygous variant in the nuclear-encoded mitochondrial protein, FBXL4 (c.1750 T > C; p.C584R) in P2. This variant was confirmed in both patients by Sanger sequencing (Fig. 1D). Of note, while the C584R variant was reported previously, along with 10 other novel *FBXL4* variants, no detailed molecular studies of the C584R variant were performed [5].

3.4. Cells homozygous for the C584R variant in FBXL4 exhibit mtDNA depletion and bioenergetic defects

Skin fibroblasts obtained from both patients were used to examine novel mitochondrial phenotypes, as well as phenotypes reported previously in fibroblasts from other FBXL4 patients [1,7–9]. Consistent with other reports, we observed 30–50% depletion of mtDNA in patient fibroblast lines (Fig. 2A). In line with these findings, we also examined mitochondrial respiration using the Seahorse analyzer. Basal respiration was reduced by 30–50% in patient fibroblasts (Fig. 2B, D). Similarly, a 30–60% decrease in maximal respiratory capacity was measured in FBXL4 patient fibroblasts (Fig. 2B, E). Of note, extracellular acidification rate (ECAR), which can reflect lactate production, showed approximately 30% increase in FBXL4 patient cells compared to controls (Fig. 2F). When we examined the expression of several subunits of OXPHOS complexes, we observed noticeably reduced expression of several OXPHOS subunits in patient cells (Fig. 2G, SupFig 1). Finally, we observed approximately 40% reduction in mitochondrial membrane potential and a 20% decrease in mitochondrial mass in both FBXL4 patient fibroblast lines (SupFig 2).

Next, we assessed mitochondrial network morphology in FBXL4 patient cells. Consistent with previous reports, cells harbouring the C584R FBXL4 mutation display noticeably fragmented mitochondrial networks (Fig. 3A, B). Additionally, we examined the levels of core mitochondrial fusion proteins (MFN1, MFN2, OPA1) in control and patient fibroblasts, but did not observe consistent changes in protein expression (Fig. 3C). However, we noted significant changes in the appearance and distribution of mtDNA nucleoids in patient cells, a feature that has been described previously in FBXL4 patient fibroblasts, but not quantified. We performed detailed quantitation of nucleoid morphology and found that on average nucleoids were ~40% larger in patient cells compared to control (Fig. 3D). Meanwhile the total number of nucleoids in patient cells was reduced by ~50% in patient cells (Fig. 3E). Qualitatively, mtDNA nucleoids showed a perinuclear distribution in FBXL4 fibroblasts, compared to a more evenly distributed nucleoids in control fibroblasts (Fig. 3A). In addition, patient cells contained many mitochondrial fragments devoid of mtDNA (Fig. 3A), which is not typical in control cells. Thus, our data indicate that the C584R variant in FBXL4 is pathogenic.

3.5. DCA reduces lactate production, but does not correct mitochondrial function

Given the reported improvements in patient symptoms following DCA administration, we examined whether DCA could reverse the mitochondrial dysfunction we observed in FBXL4 patient fibroblast lines. DCA treatment (10 mM, 24 h) was well-tolerated in control and patient fibroblasts. Notably, while DCA treatment led to a significant reduction of ECAR to control levels in both patient fibroblast lines (Fig. 2G), DCA failed to rescue mtDNA depletion or restore bioenergetic profiles (Fig. 2A–E, G). In addition, though DCA treatment promoted mitochondrial fusion in control cells, there was no change in the morphology for FBXL4 patient cells treated with DCA (Fig. 3B). Thus, despite the clinical benefits that were observed, while DCA improves ECAR, it does not seem to fix the underlying defects caused by FBXL4 impairment.

3.6. Impaired mitochondrial fusion in FBXL4 patient fibroblasts

The structural features observed in FBXL4 patient fibroblasts, including mitochondrial network fragmentation, mtDNA nucleoid clustering and overall mtDNA loss were reminiscent of the phenotypes present in cells lacking fusion [25]. In addition to the fact that DCA treatment promoted mitochondrial fusion in control cells but not in

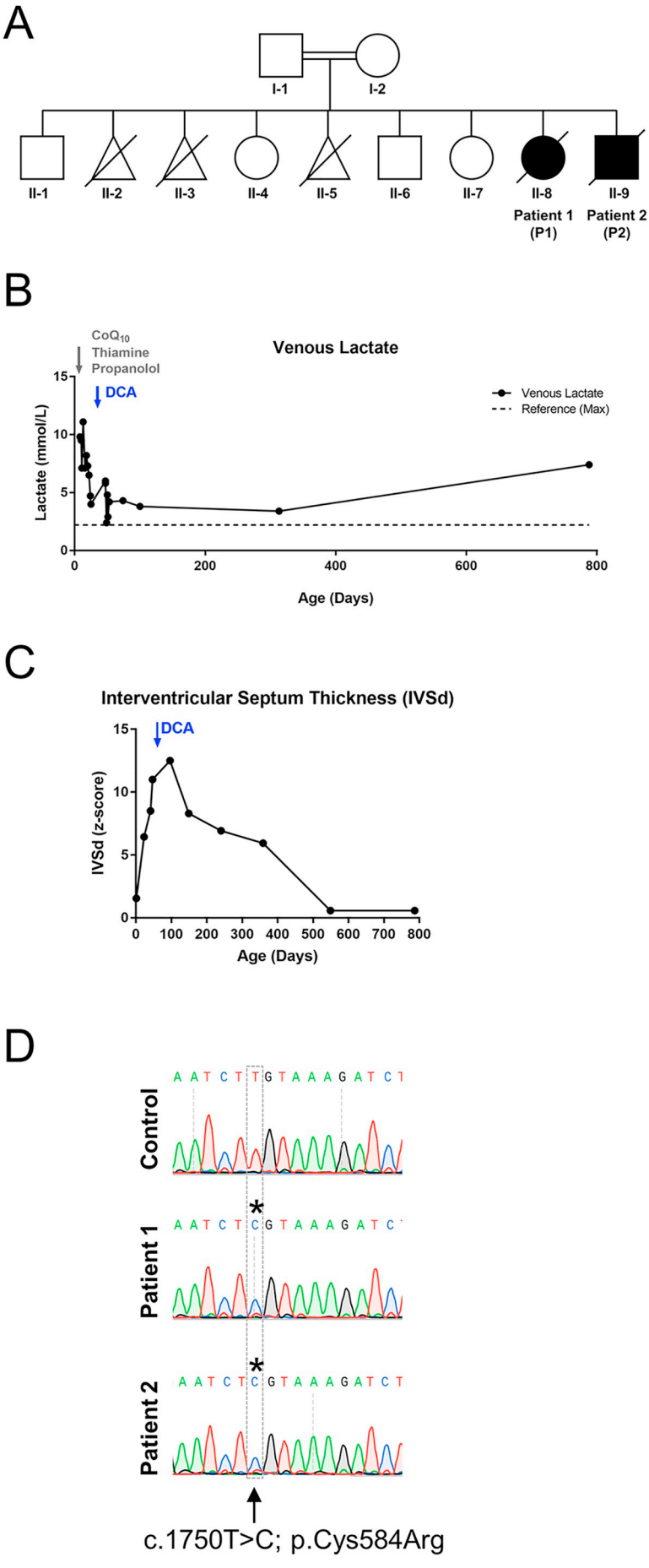

Fig. 1. Clinical investigation of mitochondrial disease patients. **A**) Family pedigree of two mitochondrial disease patients (P1 and P2) from a consanguineous marriage, both of whom presented with encephalomyopathy, severe lactic acidosis and hypertrophic cardiomyopathy. Exome sequencing of P2 identified a homozygous recessive mutation in the mitochondrial protein, FBXL4 (c. 1750 T > C; p.C584R). **B**) Increasing doses of dichloroacetate (DCA) administered to P2 around 6 weeks of age remarkably improved lactic acidosis. Dose range: 25–50 mg/kg/day. **C**) Interventricular septum thickness z-scores for P2 indicate thickening of the of the left ventricular walls which normalize after DCA administration. *Z*-scores were measured by the Boston Children's Hospital z-score calculator. **D**) Sanger sequencing of exon 9 in FBXL4 confirms the homozygous variants in P1 and P2.

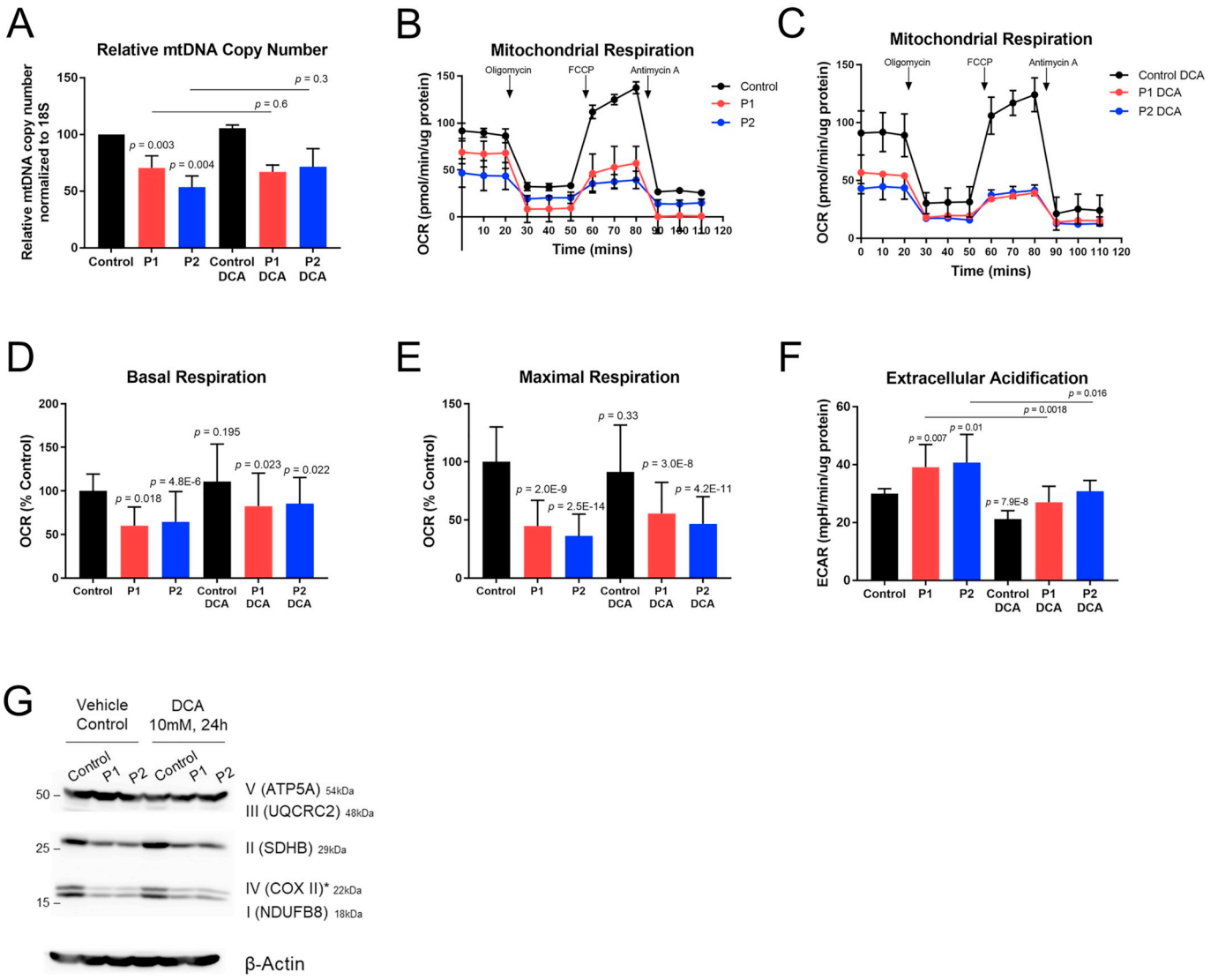

Fig. 2. Characterization of FBXL4 patient fibroblasts, and response to DCA treatment. **A**) QPCR analysis of mtDNA copy number from control and patient fibroblasts normalized to 18S. Data represents at least three independent biological replicates. **B**) Traces of oxygen consumption rates (OCR) over time analyzed in control and FBXL4 patient fibroblasts using the Seahorse XF24 extracellular flux analyzer. **C**) Traces of OCR of cells as in B following 24 h treatment with 10 mM DCA. **D**) Basal respiration in control and patient cells calculated from B and C. **E**) Maximal respiratory capacity in control and patient fibroblasts calculated from B & C. **F**) Extracellular acidification rate (ECAR) was recorded for control and patient samples treated with DCA. Data represents ECAR recordings prior to drug injections. Bioenergetic profiles were assessed from at least three technical replicates per condition. *P*-values were determined by an unpaired student *t*-test, compared to the untreated control, unless otherwise indicated. **G**) Western analysis of subunits of oxidative phosphorylation complexes in control and FBXL4 patient fibroblasts treated as indicated. MtDNA-encoded COXII of complex IV is marked with an asterisk. All other subunits are nuclear-encoded. B-actin was used as a load control. Quantification of band intensities is provided in SupFig 1.

FBXL4 patient cells, our findings led us to test the hypothesis that FBXL4 may promote mitochondrial fusion. To this end, we examined mitochondrial fusion rates in control and FBXL4 patient fibroblasts using a photo-activatable GFP (PA-GFP) fusion assay [29,35,37]. Following photoactivation of a small region of the mitochondrial network in live cells, this assay allows tracking of the diffusion of the GFP signal throughout the network as fusion of mitochondrial membranes and matrix content mixing occur. Compared to control fibroblasts, in which mitochondrial fusion was ongoing, fibroblasts with the C584R FBXL4 mutation displayed significantly reduced fusion (Fig. 4). This was quantified by two methods. First, we quantified the percentage of the photoactivated region relative to the total mitochondrial network, and measured the increase in distribution of the GFP signal over time (16 mins) (Fig. 4C, SupFig 3). The initial photo-activation region of the mitochondrial network was comparable in control and patient fibroblasts (approx. 3%). After 16 min, the GFP signal spread to about 25% of the mitochondrial network in control cells. In patient cells, however, the GFP signal spread only to 5% of the network. Secondly, we measured the relative fluorescence intensity of the GFP signal in the photo-activated region over time [35,37], where loss of signal reflects spread of the GFP signal due to fusion events (Fig. 4B, D). During the period of imaging, we observed that GFP intensity decreased by approximately 80% in control cells, compared to only 20% in FBXL4 patient cells (Fig. 4B, D). These data highlight a previously unrecognized mitochondrial fusion impairment in cells harbouring mutant FBXL4 protein.

3.7. Overexpression of wildtype FBXL4, but not C584R mutant, promotes mitochondrial fusion

We then asked whether wild-type FBXL4 could promote mitochondrial fusion. To this end, we overexpressed a C-terminal HA-tagged

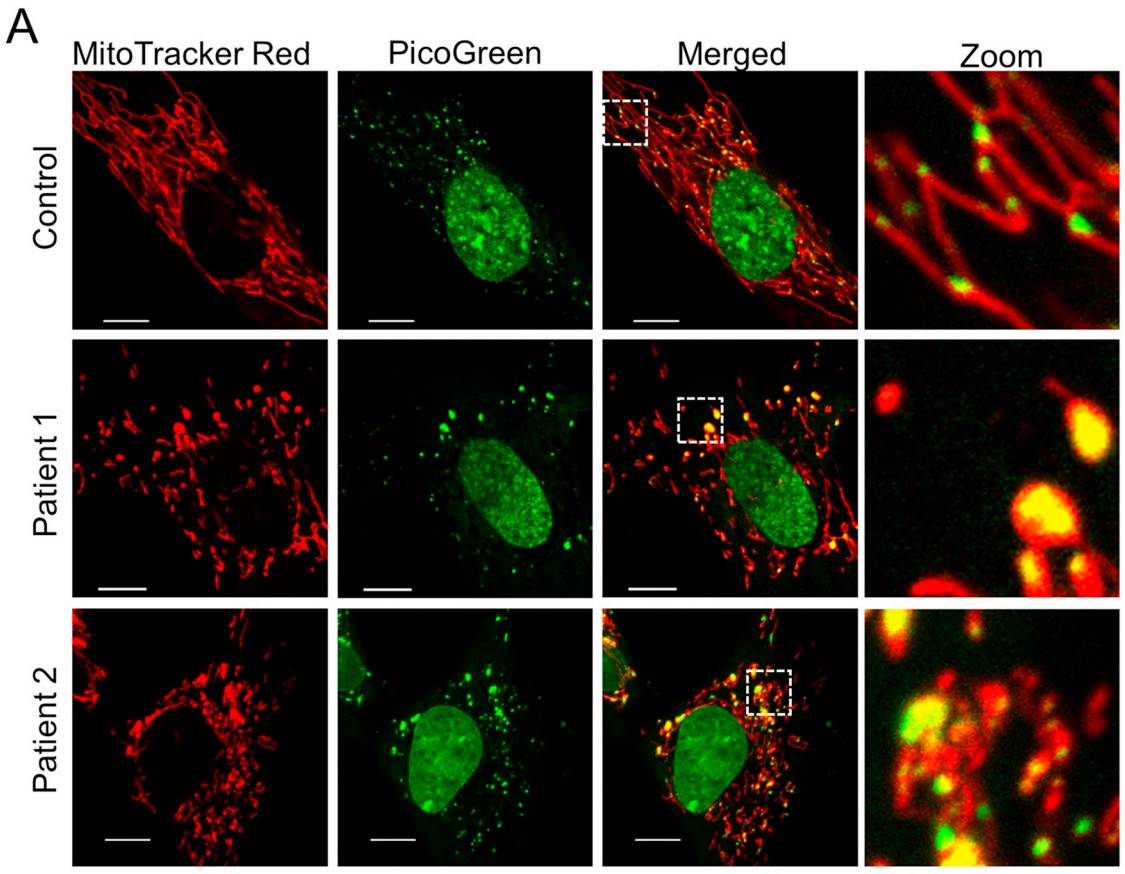

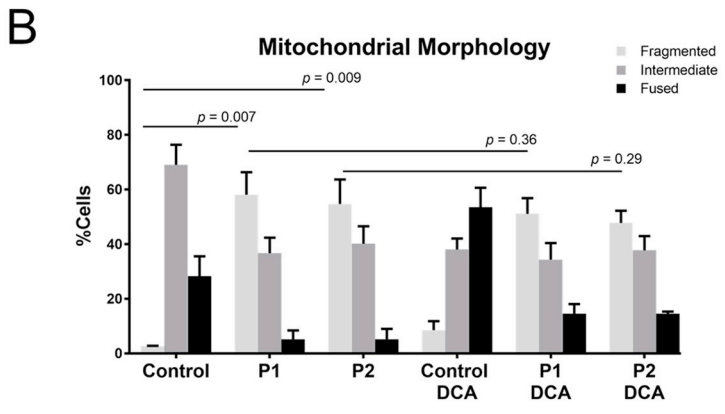

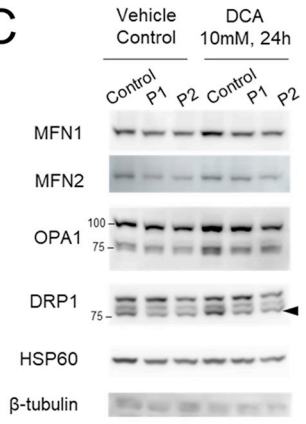

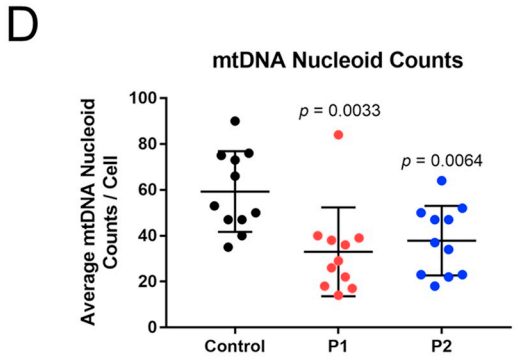

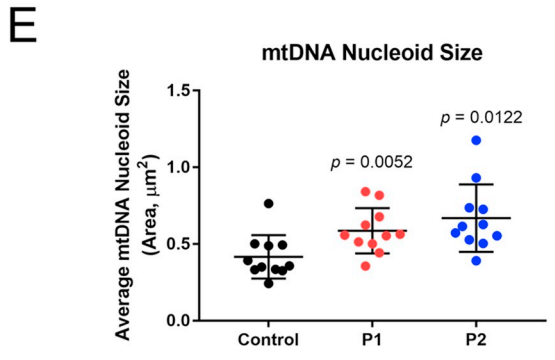

(caption on next page)

Fig. 3. Mitochondrial network and nucleoid alterations in C584R FBXL4 patient fibroblasts. **A**) Representative confocal images of control and patient cells stained with MitoTracker Red and PicoGreen (dsDNA: nuclear and mtDNA). Arrowheads in zoomed images highlight mitochondrial fragments devoid of mtDNA. Scalebars: 10 μm. **B**) Quantification of mitochondrial morphology from control and FBXL4 patient fibroblasts treated with DCA (10 mM, 24 h) or a vehicle control (DIH_2O). Morphology analysis was performed on fixed cells stained with TOMM20 from three technical replicates, quantifying at least 50 cells per fibroblast line per replicate. **C**) Western Analysis of mitochondrial fusion proteins (MFN1, MFN2, OPA1) and the main fission GTPase (DRP1) in control and patient fibroblasts treated as indicated. HSP60 and β-tubulin were used as mitochondrial and cytosolic load controls, respectively. **D**) Quantification of mtDNA nucleoid counts in control and patient fibroblasts from cells stained as in A. **E**) Quantification of mtDNA nucleoid sizes in cells stained as in A. Data represents average nucleoid sizes and counts from 10 cells for each group. *P*-values were determined by an unpaired student *t*-test, compared to the control fibroblasts.

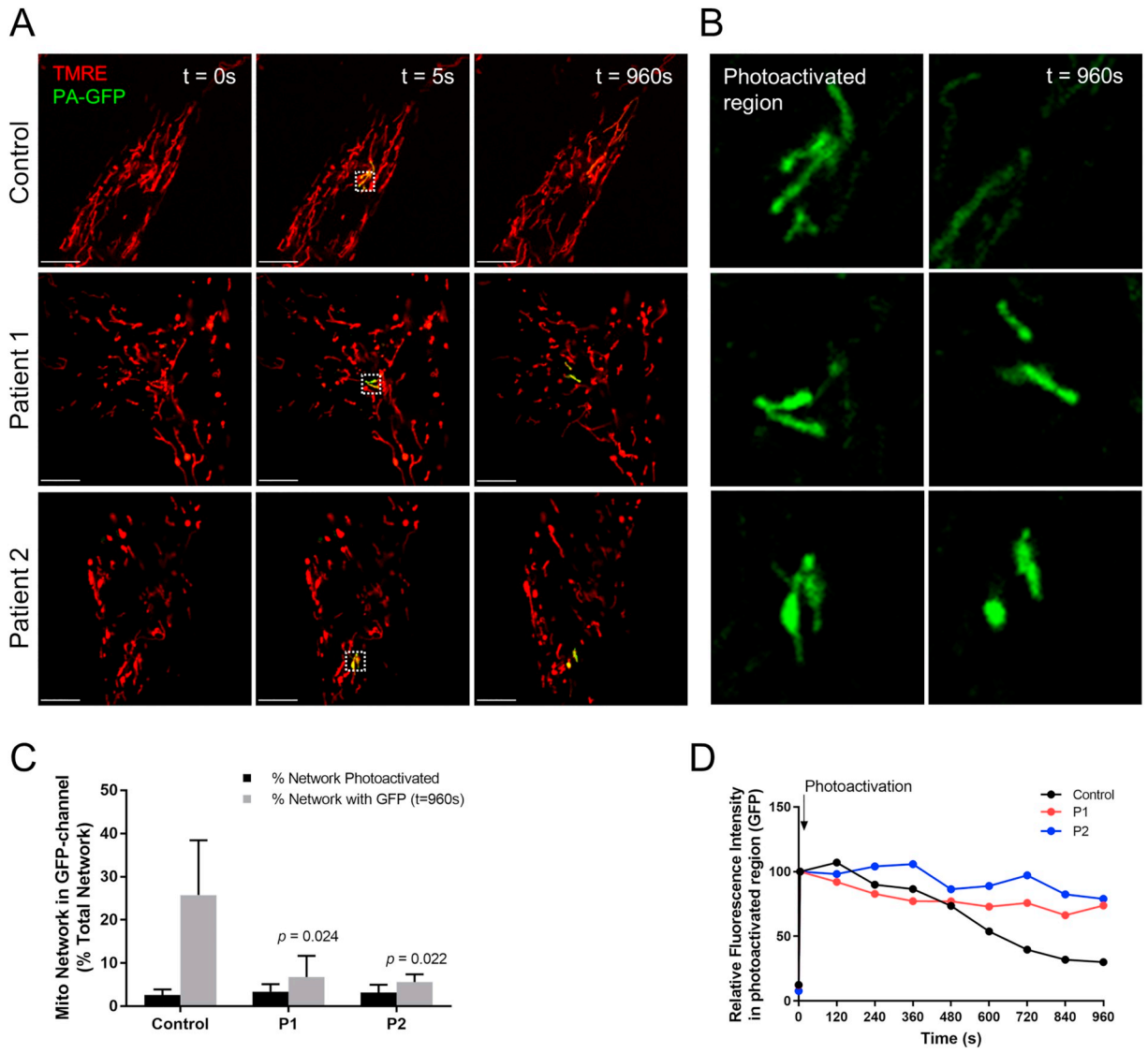

Fig. 4. Mitochondrial fusion is reduced in FBXL4 patient fibroblasts. **A**) Representative confocal images of live control and patient cells expressing a matrix-targeted PA-GFP and stained with TMRE. White boxes indicate region of photoactivation. Images were acquired pre-photoactivation, 5 s after photoactivation and then every 120 s, up to 960 s (16mins). Scalebars: 10 μm. **B**) Photoactivated region of cells shown in A, zoomed in, and showing initial photoactivate frame (t = 5 s) and final frame at 960 s. **C**) Quantification of area of photoactivated mitochondrial network at t = 5 s and the percentage of the network to which the GFP signal had spread at t = 960 s. Analysis was performed on binarized images, appended in SupFig 3. Data represent analyses in 5 cells per fibroblast line. P-values were determined by an unpaired student *t*-test, compared to the control. **D**) Relative fluorescence intensity over time in the photoactivated region indicated in panel A, at t = 0 (pre-photoactivation), t = 5 s (post-photoactivation) and 120 s intervals. Data points represent relative fluorescence intensity in the representative images shown in panel A.

FBXL4 protein in HEK cells and assessed mitochondrial network morphology 24 h post-transfection. Consistent with a role in promoting fusion, nearly 50% of HEK cells overexpressing wildtype FBXL4 contained fused mitochondrial networks, compared to ~20% in empty vector-transfected cells (Fig. 5A, B). However, overexpression of the C584R mutant FBXL4 did not lead to more cells with hyperfused mitochondrial networks (Fig. 5A, B). These findings support a novel role for FBXL4 in promoting fusion, which is abrogated by the pathogenic C584R mutation.

3.8. Restoring mitochondrial morphology in FBXL4 fibroblasts rescues mtDNA depletion

In order to determine whether impaired mitochondrial fusion is the

cause of mtDNA depletion in FBXL4 patient fibroblasts, we asked whether restoring the mitochondrial network was able to replenish levels of mtDNA. In order to restore the mitochondrial network, fibroblast cells were treated with the mitochondrial fission inhibitor mdivi-1 [38]. While we saw a trend towards an increase in mtDNA copy number in FBXL4 fibroblasts following a 24 h treatment with mdivi-1 (25 μM), this was not significant (SupFig 4). Thus, we employed a longer seven day treatment to ensure that there was enough time to allow mtDNA copy number to recover. Critically, following seven days of treatment with mdivi-1 (25 μM), we observed improved mitochondrial morphology in patient fibroblast lines and a significant increase in mtDNA copy number in FBXL4 patient fibroblasts (Fig. 6A–C).

Next, we investigated physical characteristics of mtDNA nucleoids in mdivi-1 treated fibroblasts. As an alternative approach to look at mtDNA nucleoids, we imaged mtDNA in fixed cells using and anti-DNA antibody, given that picogreen staining can sometimes be influenced by supercoiling [39]. We also used a microscope with a higher resolution and performed a z-stack in order to look at all of the nucleoids within each cell, rather than just through a single cross section of the cell. As such, the size and number of nucleoids is different than the picogreen analysis (Fig. 3). Notably, the trends for mtDNA nucleoid quantification remained the same for untreated cells, with both patient fibroblast lines exhibiting fewer but larger mtDNA nucleoids than control (Fig. 6). However, upon mdivi-1 treatment, we observed a rescue in the number of mtDNA nucleoids via microscopy in FBXL4 fibroblasts (Fig. 6D), consistent with the increased mtDNA copy number as assessed by Q-PCR. Unexpectedly, we did not observe any statistical changes in the average size of mtDNA nucleoids following mdivi-1 treatment (Fig. 6E).

4. Discussion

Mutations in the nuclear-encoded mitochondrial protein, FBXL4, are recognized to cause mtDNA depletion syndrome (over 50 mutations reported to date) [1,3–12]. However, prior to this study, the molecular function of FBXL4, and the mechanism leading to mtDNA depletion were unknown. Here, we report a previously uncharacterized variant in FBXL4 (c.1750 T > C; p.C584R) in two siblings presenting with early onset multisystemic defects including encephalomyopathy, lactic acidosis and cardiac hypertrophy. Characterization of patient-derived fibroblasts showed severe metabolic deficiencies, fragmented mitochondrial networks, fewer mtDNA nucleoids that were enlarged, as well as mtDNA depletion. Collectively, these phenotypes are consistent with previously reported pathogenic FBXL4 mutations [1,7,9] and indicate that the C584R variant is indeed pathogenic.

Given that there are many pathogenic mutations throughout the FBXL4 protein that have been described to cause the same patient phenotype [5,11], it is likely that they act as loss of function mutations. The C584R mutation investigated here lies within the leucine rich repeat (LRR) domain of FBXL4. LRR domains are known to provide a structural basis for protein-protein interactions and have been

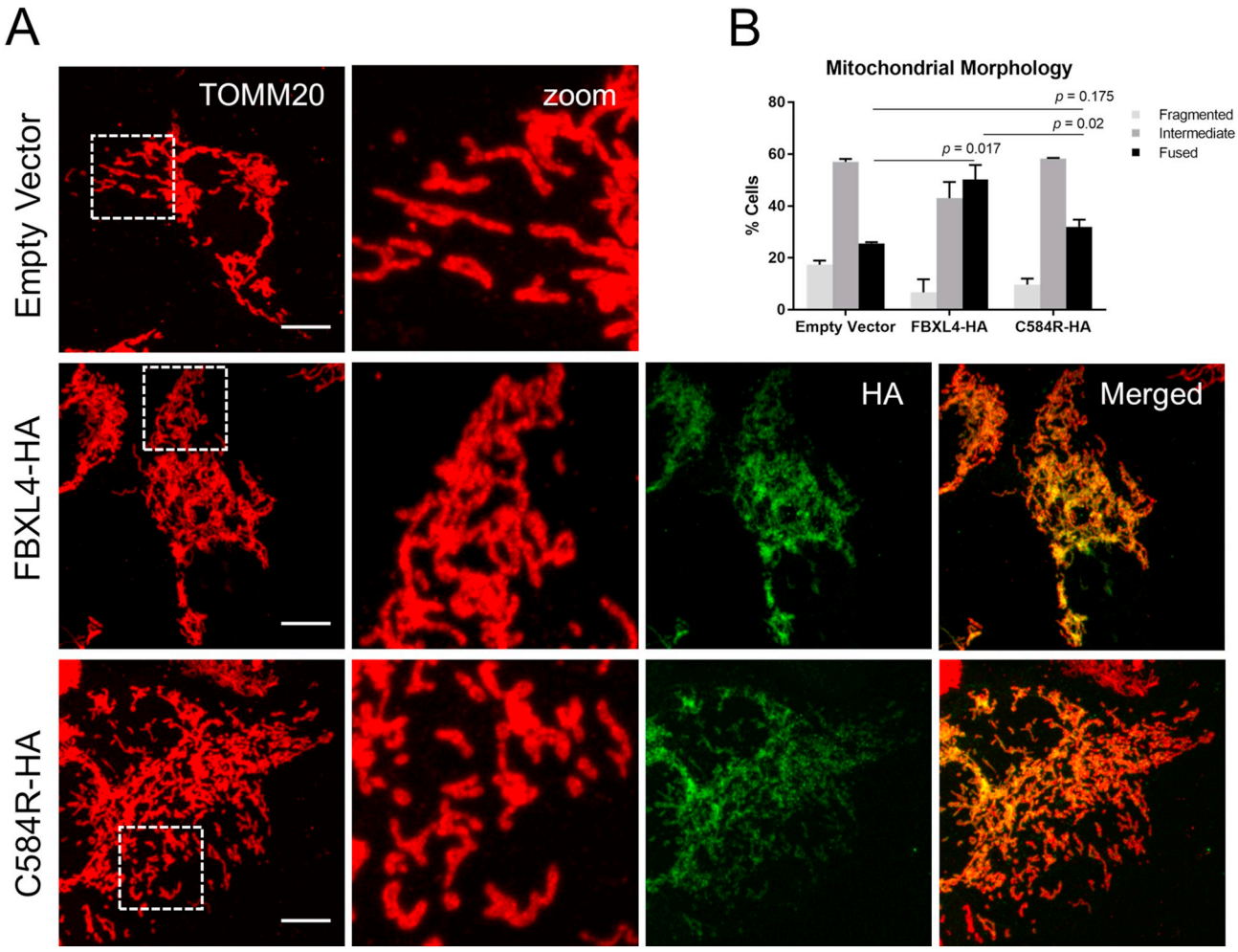

Fig. 5. FBXL4 overexpression shifts mitochondrial networks into a fused state. **A)** Representative confocal images of HEK cells transfected with an empty vector, wildtype FBXL4-HA, or C584R-HA, immunolabeled with antibodies against TOMM20 (red) and the epitope tag, HA (green). Scalebars: 10 μm. **B)** Quantification of mitochondrial morphology from cells as in panel A. P-values were determined by an unpaired student t-test, compared to the percentage of cells with a fused morphology in the indicated lines.

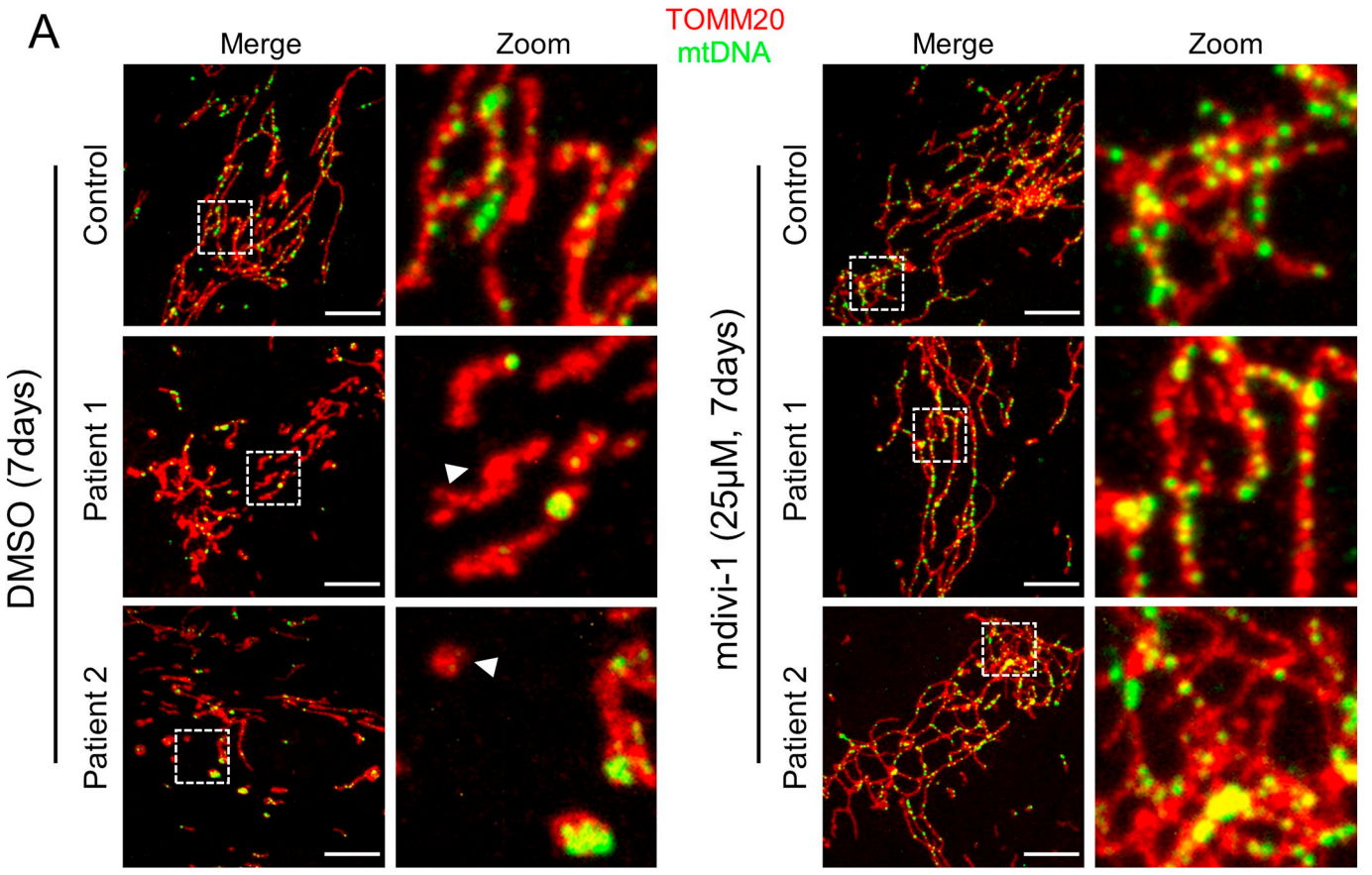

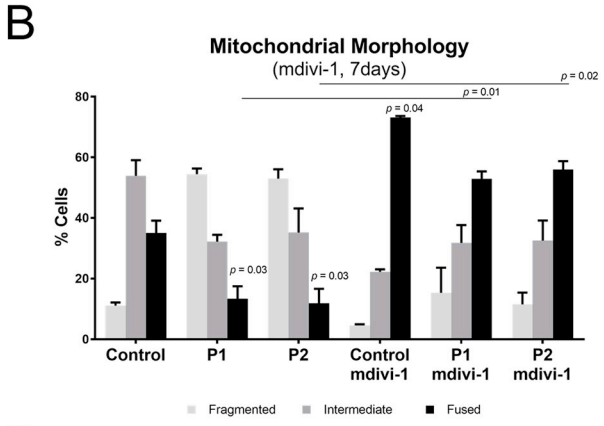

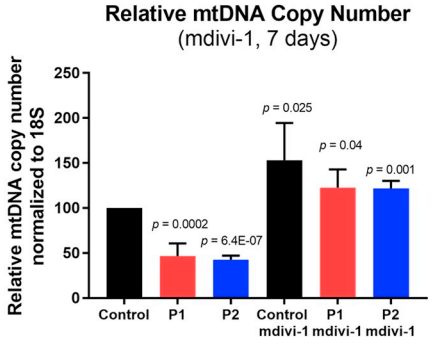

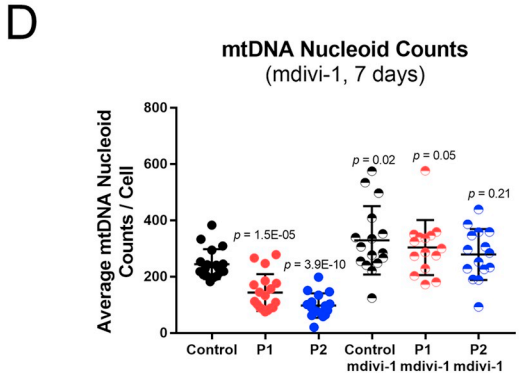

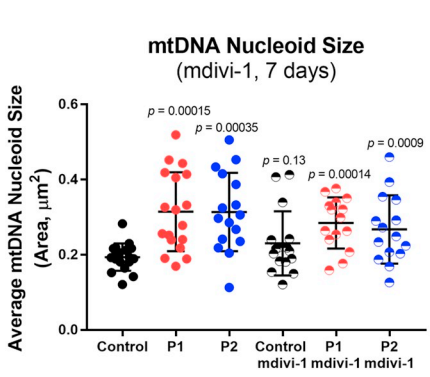

(caption on next page)

Fig. 6. Restoration of fused mitochondrial networks in FBXL4 patient fibroblasts rescues mtDNA copy number. **A**) Representative confocal images of control and patient fibroblasts treated with mdivi-1 or DMSO for 7 days, fixed and immunolabeled with antibodies against TOMM20 (red) and DNA (green). Scalebars: 10 μm. B) Mitochondrial morphology analysis of control and patient cells treated with mdivi-1 or a vehicle control for 7 days. Data represents two independent biological replicates. C) Relative mtDNA copy number in control and patient cells treated with mdivi-1 or a vehicle control for 7 days. D) Average mtDNA nucleoid counts from cells treated as indicated, fixed and immunolabeled with an anti-DNA antibody. E) Average mtDNA nucleoid sizes from cells as in D. P-values were determined by an unpaired student *t*-test, comparing each group to the vehicle control-treated control fibroblasts.

implicated in a diverse array of functions [40]. Given the amino acid change from cysteine, with a polar side chain containing a reactive sulfhydryl group that can form disulfide bonds, to arginine, with a basic positively charged side chain, it is possible that the structure of the LRR is altered such that it prevents normal protein-protein interactions required for FBXL4 to promote mitochondrial fusion.

Congenital lactic acidosis has been reported in all patients carrying pathogenic variants in FBXL4 to date [1,3–12]. However, there have not been any reports of effective interventions for lactic acidosis in these patients. Notably, DCA was administered to P2 at 6 weeks of age. In response to DCA treatment venous lactate levels were reduced, and a remarkable reversal of the cardiac hypertrophy was noted. Importantly, the prolonged survival for P2 (2 years and 10 months) is also notable, compared to P1 carrying the same mutation, who passed at 7 months of age. Thus, we set out to leverage these positive clinical outcomes and ask whether DCA could reverse mitochondrial dysfunction in FBXL4 patient fibroblasts. Consistent with the known mechanism of action for DCA, extracellular acidification was reversed in patient cells. However, none of the other parameters of mitochondrial dysfunction we investigated were improved by DCA treatment. This finding suggests that the clinical benefits reported for DCA encompass managing only the lactic acidosis, while the underlying mechanism causing mitochondrial dysfunction was not resolved by DCA. The fact that DCA also reversed the cardiovascular dysfunction in P2, suggests that the increase in lactate specifically was most likely responsible for the cardiovascular dysfunction in this patient.

Though rare, normalization of cardiac dysfunction in mitochondrial disease patients has been reported previously [41]. Notably, in a patient with lactic acidosis and hypertrophic cardiomyopathy, who harbored pathogenic mutations in the mitochondrial translation optimization 1 protein (MTO1) [42,43], DCA treatment was also beneficial, and correlated with reduced lactate levels and reversal of cardiac dysfunction. A continued regimen of DCA and co-factors was suggested to have prolonged survival in this MTO1 patient into adulthood [43]. In these rare cases, restoration of cardiac function occurs in patients surviving past one year of age. Together with our FBXL4 patient, these observations suggest that there is a critical developmental period early in life, where high levels of lactate are detrimental to cardiac function.

While DCA has been used to treat mitochondrial disease in the past, patients' responses have been extremely variable, and DCA can even be deleterious. Positive clinical outcomes following DCA treatment have been reported in several studies involving patients with lactic acidosis [42–46]. Chronic DCA administration, in patients with congenital causes of lactic acidosis (deficiencies of PDHC, Respiratory chain complex I, IV or I + IV), into adulthood has been reported to be tolerable and beneficial at maintaining blood lactate levels [42,43,46]. Meanwhile, a clinical trial examining the efficacy of DCA in mitochondrial myopathy, encephalopathy, lactic acidosis and stroke-like episodes (MELAS) patients was prematurely terminated due peripheral nerve toxicity in 17/19 participants [47]. As such, clinical use of DCA has declined and it has orphan drug status [48,49]. The variability in outcomes of mitochondrial disease patients treated with DCA likely reflects the genetic and phenotypic heterogeneity of mitochondrial diseases in general. To this end, we argue that the use of DCA to manage elevated blood lactate should be practiced with caution, considering the underlying pathogenesis mechanism leading to lactatemia. Importantly, DCA treatment may be a viable option to manage symptoms in mitochondrial disease patients presenting with pathogenic variants in FBXL4.

In order to understand how mutations in FBXL4 cause mtDNA depletion, we sought to investigate the molecular function of FBXL4 in mitochondria. Considering the mechanisms known to lead to mtDNA depletion, we reasoned that FBXL4, proposed as an IMS protein [1], would be unlikely to directly regulate replication and maintenance of mitochondrial genomes localized in the matrix [22]. Moreover, the mitochondrial fragmentation and enlarged mtDNA nucleoids that we and others observed in FBXL4 patient fibroblasts were particularly intriguing [1,7,9]. Together with the mtDNA depletion phenotype, these features have also been reported in cells lacking mitochondrial fusion [15,16,25,50]. Additionally, the fact that DCA promoted fused mitochondrial networks in control fibroblasts, but not in FBXL4 patient cells, also suggested an impairment in the dynamic regulation of mitochondrial structure. Hence, we speculated that FBXL4 had a previously unrecognized role in promoting mitochondrial fusion.

Our study is the first to demonstrate that FBXL4 promotes mitochondrial fusion. We found that mitochondrial fusion rates were greatly reduced in FBXL4 patient fibroblast cells, which explains the fragmented mitochondrial networks and enlarged mtDNA nucleoids in these cells. In fact, our observations in FBXL4 patient fibroblasts were comparable to impaired fusion in MFN2 knockout mouse embryonic fibroblasts described previously [29]. Moreover, overexpression of FBXL4 led to a marked increase in the number of cells with reticular mitochondrial networks, demonstrating that FBXL4 promotes mitochondrial fusion. Finally, the C584R mutation abrogates the pro-fusion activity of FBXL4. Taken together, these results demonstrate a novel role for FBXL4 in promoting mitochondrial fusion. The exact mechanism through which FBXL4 protein promotes fusion is still an open area for investigation. Notably, it is intriguing that the total amounts of fusion proteins (MFN1/2 and OPA1) are largely unaltered in FBXL4 patient cells compared to control, which suggests that the lower fusion rates are not due to reduced stability of fusion GTPases, but by some other mechanism. Future work studying how FBXL4 promotes fusion could lead to new approaches to mediate mitochondrial dynamics as a therapeutic approach for a growing list of pathologies where mitochondrial fragmentation is implicated [51–53].

Our data also suggest that the reduction in mitochondrial fusion is the most likely explanation for why FBXL4 impairments causes mtDNA depletion and disease. When we restored the mitochondrial network to a more fused state in patient fibroblasts, we observed a rescue of both the mtDNA copy number and the number of mtDNA nucleoids. If the mtDNA depletion had been due to reduced levels of mitochondrial dNTP nucleotide pools, then mdivi-1 treatment should not have rescued the mtDNA copy number. Our finding that restoring the network morphology rescued mtDNA copy number in FBXL4 fibroblasts is consistent with recent work showing that a fused network is important for proper distribution of the mtDNA replisome components in order to maintain mtDNA copy number [54]. It is also notable that restoring the mitochondrial network does not immediately rescue the mtDNA copy number, suggesting it takes > 1 day for copy number to be re-established following restoration of the mitochondrial network.

Unexpectedly, we did not see a rescue of the mtDNA nucleoid size at seven days, suggesting that there may not be a direct correlation between nucleoid clumping and mtDNA copy number. However, this lack of rescue could be due to the fact that large nucleoids persist longer than seven days. Alternatively, mdivi-1 treatment has been shown to induce nucleoid clumping [24], which is potentially a confounding

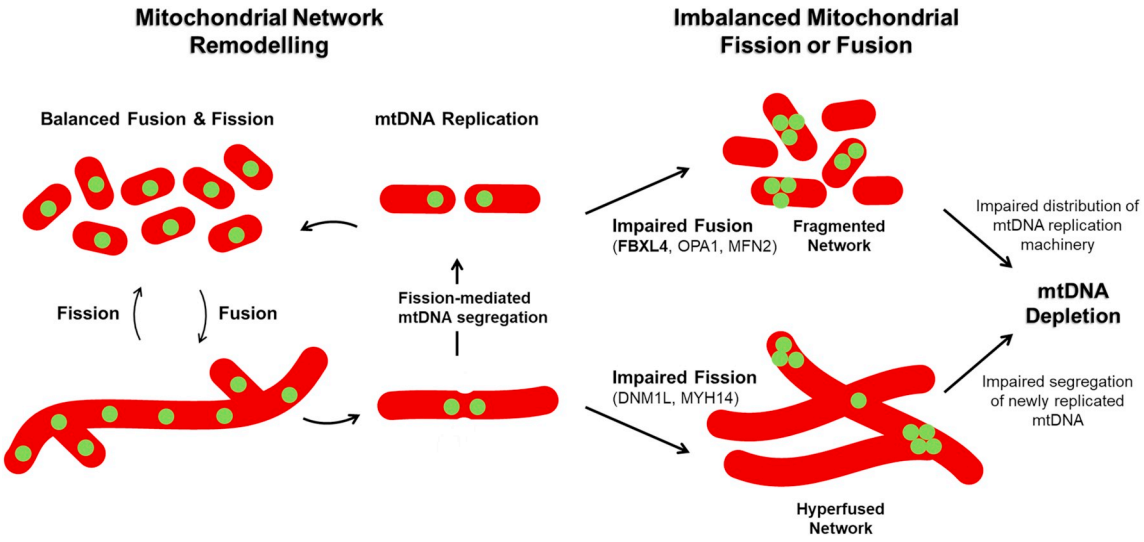

Fig. 7. Proposed model for mtDNA depletion and altered nucleoids distribution in cells with impaired mitochondrial dynamics regulation. Under normal conditions, balanced fusion and fission events ensure even distribution of mtDNA nucleoids throughout reticular mitochondrial networks or fragmented puncta. Notably, mitochondrial fission at sites of mtDNA replication facilitates segregation of newly synthesized mtDNA, thus maintaining mtDNA copies throughout the network. An imbalance in mitochondrial dynamics, arising from impaired fusion (e.g. in mutant FBXL4, OPA1 or MFN2), leads to excessive fragmentation of the mitochondrial network, clustering of mtDNA nucleoids and mtDNA depletion. Meanwhile, in cells with defective fission (e.g. mutant DNM1L, MYH14), mtDNA nucleoids form large aggregates due to inefficient segregation following replication, which may contribute to mtDNA depletion.

factor. Although it should be noted that we did not see a significant increase in nucleoid size in control fibroblasts following seven days of mdivi-1 treatment. Thus, at this juncture we cannot make any definitive conclusions regarding the correlation between mtDNA nucleoid clumping and mtDNA depletion. Nonetheless, it is intriguing that loss of the mitochondrial fission protein Drp1 has also been shown to lead to larger mtDNA nucleoids and mtDNA depletion [24,55]. Meanwhile, a pathogenic mutation in MYH14, encoding a myosin protein recently implicated in mitochondrial fission, also leads to hyperfused mitochondrial networks and larger mtDNA nucleoids [56]. In this context, recent work suggests that mitochondrial fission is important to segregate newly synthesized mtDNA nucleoids [57,58]. However, exactly how loss of fusion relates to clumping of mtDNA nucleoids remains unresolved (Fig. 7).

Collectively, our data highlight impaired mitochondrial fusion as the most likely mechanism underlying pathogenic mtDNA depletion caused by mutations in *FBXL4*. Identifying FBXL4 as a novel protein promoting mitochondrial fusion adds mechanistic insight into the field of mitochondrial dynamics, particularly given the importance of mitochondrial fusion in health and disease. Thus, future studies are warranted in order to develop a comprehensive mechanistic understanding of FBXL4 as a pro-fusion factor. Finally, though our research suggests that DCA may be an effective treatment option to help deal with elevated lactate levels in patients with mutations in *FBXL4*, DCA does not restore FBXL4 function. Nonetheless, novel therapeutic approaches to restore mitochondrial morphology may be beneficial for patients with FBXL4 dysfunction.

Funding

This work was performed under the Care4Rare Canada Consortium funded by Genome Canada, the Canadian Institutes of Health Research, the Ontario Genomics Institute, Ontario Research Fund, Genome Alberta, Genome British Columbia, Genome Quebec, and Children's Hospital of Eastern Ontario Foundation. This work was supported by funds provided by the Alberta Children's Hospital Research Institute (ACHRI), the Alberta Children's Hospital Foundation and the Natural Sciences and Engineering Research Council of Canada (NSERC - RGPIN-2016-04083) (T.S.). R.S. is a recipient of a Queen Elizabeth II Graduate Scholarship and ACHRI Graduate Studentship. A.K. received research funding from Mito Canada. The funding sources were not involved in the study design, data collection and analysis, the writing of the report, nor in the decision to submit.

Transparency document

The Transparency document associated with this article can be found, in online version.

CRediT authorship contribution statement

Rasha Sabouny: Conceptualization, Formal analysis, Methodology, Writing - original draft, Writing - review & editing. **Rachel Wong:** Methodology. **Laurie Lee-Glover:** Methodology. **Steven C. Greenway:** Investigation, Writing - review & editing. **David S. Sinasac:** Conceptualization, Investigation, Writing - review & editing. **Aneal Khan:** Conceptualization, Investigation, Supervision, Writing - review & editing. **Timothy E. Shutt:** Conceptualization, Supervision, Writing - original draft, Writing - review & editing.

Acknowledgments

We are grateful to Dr. Massimo Zeviani for generously sharing FBXL4-HA constructs. We would also like to acknowledge Dr. Laurie Kennedy and Dr. Yiping Liu at the Flow Cytometry Facility, University of Calgary.

Appendix A. Supplementary data

Supplementary data to this article can be found online at https://doi.org/10.1016/j.bbadis.2019.165536.

References

[1] X. Gai, et al., Mutations in FBXL4, encoding a mitochondrial protein, cause early-onset mitochondrial encephalomyopathy, Am. J. Hum. Genet. 93 (3) (2013) 482–495.
[2] J.S. Amberger, et al., OMIM.org: Online Mendelian Inheritance in Man (OMIM(R)), an online catalog of human genes and genetic disorders, Nucleic Acids Res. 43

(Database issue) (2015) D789–D798.
[3] C. Kuptanon, et al., Whole exome sequencing revealed mutations in FBXL4, UNC80, and ADKin Thai patients with severe intellectual disabilities, Gene 696 (2019) 21–27, https://doi.org/10.1016/j.gene.2019.01.049.
[4] M. Huemer, et al., Clinical, morphological, biochemical, imaging and outcome parameters in 21 individuals with mitochondrial maintenance defect related to FBXL4 mutations, J. Inherit. Metab. Dis. 38 (5) (2015) 905–914.
[5] A.W. El-Hattab, et al., Molecular and clinical spectra of FBXL4 deficiency, Hum. Mutat. 38 (12) (2017) 1649–1659.
[6] D. Ebrahimi-Fakhari, et al., Recurrent stroke-like episodes in FBXL4-associated early-onset mitochondrial encephalomyopathy, Pediatr. Neurol. 53 (6) (2015) 549–550.
[7] P.E. Bonnen, et al., Mutations in FBXL4 cause mitochondrial encephalopathy and a disorder of mitochondrial DNA maintenance, Am. J. Hum. Genet. 93 (3) (2013) 471–481.
[8] T. Baroy, et al., A novel mutation in FBXL4 in a Norwegian child with encephalomyopathic mitochondrial DNA depletion syndrome 13, Eur. J. Med. Genet. 59 (6–7) (2016) 342–346.
[9] G. Antoun, et al., Detailed Biochemical and Bioenergetic Characterization of FBXL4-Related Encephalomyopathic Mitochondrial DNA Depletion, JIMD Rep (2015).
[10] S.U. Morton, et al., Hyperammonemia as a presenting feature in two siblings with FBXL4 variants, JIMD Rep. 35 (2017) 7–15.
[11] H. Dai, et al., FBXL4 defects are common in patients with congenital lactic acidemia and encephalomyopathic mitochondrial DNA depletion syndrome, Clin. Genet. 91 (4) (2017) 634–639.
[12] R.A. Ballout, et al., FBXL4-related mitochondrial DNA depletion syndrome 13 (MTDPS13): a case report with a comprehensive mutation review, Front. Genet. (2019) 10(39).
[13] A. Suomalainen, P. Isohanni, Mitochondrial DNA depletion syndromes—many genes, common mechanisms, Neuromuscul. Disord. 20 (7) (2010) 429–437.
[14] A.W. El-Hattab, F. Scaglia, Mitochondrial DNA depletion syndromes: review and updates of genetic basis, manifestations, and therapeutic options, Neurotherapeutics 10 (2) (2013) 186–198.
[15] S. Vielhaber, et al., Mitofusin 2 mutations affect mitochondrial function by mitochondrial DNA depletion, Acta Neuropathol. 125 (2) (2013) 245–256.
[16] R. Spiegel, et al., Fatal infantile mitochondrial encephalomyopathy, hypertrophic cardiomyopathy and optic atrophy associated with a homozygous OPA1 mutation, J. Med. Genet. 53 (2) (2016) 127–131.
[17] P. Amati-Bonneau, et al., OPA1 mutations induce mitochondrial DNA instability and optic atrophy 'plus' phenotypes, Brain 131 (Pt 2) (2008) 338–351.
[18] J.Y. Kim, et al., Mitochondrial DNA content is decreased in autosomal dominant optic atrophy, Neurology 64 (6) (2005) 966–972.
[19] F. Renaldo, et al., MFN2, a new gene responsible for mitochondrial DNA depletion, Brain 135 (Pt 8) (2012) e223 (1–4; author reply e224, 1–3).
[20] S.L. Archer, Mitochondrial dynamics–mitochondrial fission and fusion in human diseases, N. Engl. J. Med. 369 (23) (2013) 2236–2251.
[21] T.E. Shutt, H.M. McBride, Staying cool in difficult times: mitochondrial dynamics, quality control and the stress response, Biochim. Biophys. Acta 1833 (2) (2013) 417–424.
[22] T.J. Nicholls, C.M. Gustafsson, Separating and segregating the human mitochondrial genome, Trends Biochem. Sci. 43 (11) (2018) 869–881.
[23] C.M. Gustafsson, M. Falkenberg, N.G. Larsson, Maintenance and expression of mammalian mitochondrial DNA, Annu. Rev. Biochem. 85 (2016) 133–160.
[24] R. Ban-Ishihara, et al., Dynamics of nucleoid structure regulated by mitochondrial fission contributes to cristae reformation and release of cytochrome c, Proc. Natl. Acad. Sci. U. S. A. 110 (29) (2013) 11863–11868.
[25] H. Chen, J.M. McCaffery, D.C. Chan, Mitochondrial fusion protects against neurodegeneration in the cerebellum, Cell 130 (3) (2007) 548–562.
[26] T. Wai, T. Langer, Mitochondrial dynamics and metabolic regulation, Trends Endocrinol. Metab. 27 (2) (2016) 105–117, https://doi.org/10.1016/j.tem.2015.12.001.
[27] S. Whitehouse, R.H. Cooper, P.J. Randle, Mechanism of activation of pyruvate dehydrogenase by dichloroacetate and other halogenated carboxylic acids, Biochem. J. 141 (3) (1974) 761–774.
[28] P.W. Stacpoole, The pharmacology of dichloroacetate, Metabolism 38 (11) (1989) 1124–1144.
[29] M. Karbowski, M.M. Cleland, B.A. Roelofs, Photoactivatable green fluorescent protein-based visualization and quantification of mitochondrial fusion and mitochondrial network complexity in living cells, Methods Enzymol. 547 (2014) 57–73.
[30] J.S. Eaton, et al., Ataxia-telangiectasia mutated kinase regulates ribonucleotide reductase and mitochondrial homeostasis, J. Clin. Invest. 117 (9) (2007) 2723–2734.
[31] K.J. Livak, T.D. Schmittgen, Analysis of relative gene expression data using real-time quantitative PCR and the 2(−Delta Delta C(T)) method, Methods 25 (4) (2001) 402–408.
[32] R. Sabouny, et al., The Keap1-Nrf2 stress response pathway promotes mitochondrial hyperfusion through degradation of the mitochondrial fission protein Drp1, Antioxid. Redox Signal. 27 (18) (2017) 1447–1459.
[33] N. Ashley, D. Harris, J. Poulton, Detection of mitochondrial DNA depletion in living human cells using PicoGreen staining, Exp. Cell Res. 303 (2) (2005) 432–446.
[34] J. Schindelin, et al., Fiji: an open-source platform for biological-image analysis, Nat. Methods 9 (7) (2012) 676–682.
[35] A.J. Molina, O.S. Shirihai, Monitoring mitochondrial dynamics with photo-activatable [corrected] green fluorescent protein, Methods Enzymol. 457 (2009) 289–304.
[36] H.B. Sarnat, et al., Endothelial ultrastructural alterations of intramuscular capillaries in infantile mitochondrial cytopathies: "mitochondrial angiopathy", Neuropathology 32 (6) (2012) 617–627.
[37] A. Lovy, et al., A faster, high resolution, mtPA-GFP-based mitochondrial fusion assay acquiring kinetic data of multiple cells in parallel using confocal microscopy, J. Vis. Exp. 65 (2012) e3991.
[38] A. Cassidy-Stone, et al., Chemical inhibition of the mitochondrial division dynamin reveals its role in Bax/Bak-dependent mitochondrial outer membrane permeabilization, Dev. Cell 14 (2) (2008) 193–204.
[39] J. He, et al., The AAA+ protein ATAD3 has displacement loop binding properties and is involved in mitochondrial nucleoid organization, J. Cell Biol. 176 (2) (2007) 141–146.
[40] B. Kobe, A.V. Kajava, The leucine-rich repeat as a protein recognition motif, Curr. Opin. Struct. Biol. 11 (6) (2001) 725–732.
[41] V. Boczonadi, B. Bansagi, R. Horvath, Reversible infantile mitochondrial diseases, J. Inherit. Metab. Dis. 38 (3) (2015) 427–435.
[42] D. Ghezzi, et al., Mutations of the mitochondrial-tRNA modifier MTO1 cause hypertrophic cardiomyopathy and lactic acidosis, Am. J. Hum. Genet. 90 (6) (2012) 1079–1087.
[43] E. Baruffini, et al., MTO1 mutations are associated with hypertrophic cardiomyopathy and lactic acidosis and cause respiratory chain deficiency in humans and yeast, Hum. Mutat. 34 (11) (2013) 1501–1509.
[44] P.W. Stacpoole, et al., Controlled clinical trial of dichloroacetate for treatment of congenital lactic acidosis in children, Pediatrics 117 (5) (2006) 1519–1531.
[45] B.A. Barshop, et al., Chronic treatment of mitochondrial disease patients with dichloroacetate, Mol. Genet. Metab. 83 (1–2) (2004) 138–149.
[46] M. Abdelmalak, et al., Long-term safety of dichloroacetate in congenital lactic acidosis, Mol. Genet. Metab. 109 (2) (2013) 139–143.
[47] P. Kaufmann, et al., Dichloroacetate causes toxic neuropathy in MELAS: a randomized, controlled clinical trial, Neurology 66 (3) (2006) 324–330.
[48] S. Parikh, et al., A modern approach to the treatment of mitochondrial disease, Curr. Treat. Options Neurol. 11 (6) (2009) 414–430.
[49] S. Avula, et al., Treatment of mitochondrial disorders, Curr. Treat. Options Neurol. 16 (6) (2014) 292.
[50] G. Elachouri, et al., OPA1 links human mitochondrial genome maintenance to mtDNA replication and distribution, Genome Res. 21 (1) (2011) 12–20.
[51] W.X. Tang, et al., Early protective effect of mitofusion 2 overexpression in STZ-induced diabetic rat kidney, Endocrine 41 (2) (2012) 236–247.
[52] A. Jahani-Asl, et al., The mitochondrial inner membrane GTPase, optic atrophy 1 (Opa1), restores mitochondrial morphology and promotes neuronal survival following excitotoxicity, J. Biol. Chem. 286 (6) (2011) 4772–4782.
[53] H. Chen, D.C. Chan, Mitochondrial dynamics—fusion, fission, movement, and mitophagy—in neurodegenerative diseases, Hum. Mol. Genet. 18 (R2) (2009) R169–R176.
[54] E. Silva Ramos, et al., Mitochondrial fusion is required for regulation of mitochondrial DNA replication, PLoS Genet. 15 (6) (2019) e1008085.
[55] T. Ishihara, et al., Dynamics of mitochondrial DNA nucleoids regulated by mitochondrial fission is essential for maintenance of homogeneously active mitochondria during neonatal heart development, Mol. Cell. Biol. 35 (1) (2015) 211–223.
[56] W. Almutawa, et al., The R941L mutation in MYH14 disrupts mitochondrial fission and associates with peripheral neuropathy, EBioMedicine 45 (2019) 379–392, https://doi.org/10.1016/j.ebiom.2019.06.018.
[57] S.C. Lewis, L.F. Uchiyama, J. Nunnari, ER-mitochondria contacts couple mtDNA synthesis with mitochondrial division in human cells, Science 353 (6296) (2016) aaf5549.
[58] T.J. Nicholls, et al., Topoisomerase 3alpha is required for decatenation and segregation of human mtDNA, Mol. Cell 69 (1) (2018) 9–23 (e6).